Supporting Information

Nori et al. 10.1073/pnas.1108077108

SI Materials and Methods

Behavioral Analyses. The locomotor performance of mice was analyzed using the Basso mouse scale (BMS) score for 56 or 112 d (1). The BMS score was determined for 28 mice in the hiPSC-NS group and 26 mice in the control group for up to 56 d after spinal cord injury (SCI). Thereafter, the BMS score was observed for 18 mice in the hiPSC-NS group and 16 mice in the control group, until 112 d after SCI.

Motor coordination was assessed with a rotating rod (Rotarod) apparatus (Muromachi Kikai), consisting of a plastic rod (3-cm diameter, 8-cm length) with a gritted surface, flanked by two large discs (40-cm diameter). Fifty-six days after SCI, each mouse was placed on the rod, and the rod was rotated at 20 rpm. Latency until falling was monitored for 120 s (2, 3). Two trials were conducted, and the average number of seconds was recorded. Ten mice each from the hiPSC-NS and control groups were used in the Rotarod test.

Gait analysis was performed using the DigiGait system (Mouse Specifics) (4, 5). Briefly, digital images of paw placement were recorded at 80 Hz through a clear treadmill from below the animal. Mice were tested in one session without pretraining at a speed of 8 cm/s. In this method, the area of each digital paw print is imaged sequentially, providing a dynamic gait signal. A plot of these areas represents the record of paw placement relative to the treadmill belt over time. Stride length is calculated from the fixed walking speed divided by the measured stride frequency (strides per second). Data were collected for the DigiGait system on day 56 after SCI, when mice demonstrated consistent weight-supported hindlimb stepping on the treadmill at 8 cm/s. Treadmill gait analysis was performed for 18 mice in the hiPSC-NS group and 16 in the control group.

All evaluations were made by two observers blinded to the identity of the mouse group analyzed.

Electrophysiology. For the electrophysiological experiments (MEB-9402; Nihon Kohden), mice were given an i.p. injection of ketamine (100 mg/kg) and xylazine (10 mg/kg), and 10 square-wave stimuli of 0.2-ms duration with a stimulus intensity of 0.4 mA and an interstimulus interval of 1 Hz were delivered through the occipitocervical area of the spinal cord and hindlimb by needle electrodes. The active electrode was placed in the muscle belly, and the reference electrode was placed near the distal tendon of the muscle in the hindlimb. The ground electrode was placed s.c. on the tail. Electrophysiological analysis was performed for 17 mice in the hiPSC-NS group and 15 in the control group. The onset latency was measured as the length of time in milliseconds between the stimulus and the onset of the first wave. Ten responses in each mouse were averaged for the latency analysis. Electrophysiology was performed as in a previous study (6) with the following modifications: the occipitocervical area of the spinal cord was directly stimulated with a stimulus intensity of 0.4 mA.

Histological and Cytological Analyses. Mice were deeply anesthetized and transcardially perfused with 4% paraformaldehyde, 56 (n = 10, each group) or 112 d (n = 18 hiPSC-NS group; n = 16, control group) after SCI, for histological analyses. Dissected spinal cords were postfixed overnight in 4% PFA, soaked overnight in 10% followed by 30% sucrose, embedded in OCT compound (Sakura Finetechnical), and sectioned in the sagittal or axial plane at 12 μm on a cryostat (CM3050 S; Leica). The injured spinal cords were histologically evaluated by hematoxylin–eosin (H&E) staining, Luxol fast blue (LFB) staining, and immunohistochemistry.

Tissue sections were stained with the following primary antibodies: anti-GFP (rabbit IgG, 1:200; Frontier Institute), anti-GFP (goat IgG, 1:200; Rockland), anti–β-tubulin isotype III (βIII tubulin, mouse IgG, 1:1,000; Sigma), antihuman nuclear protein antibody (HNu, mouse IgG, 1:500; Chemicon), antineuronal nuclei (NeuN, mouse IgG, 1:200; Chemicon), antiglial fibrillary acidic protein (GFAP, rabbit IgG, 1:200; Dako), anti-GFAP (guinea pig IgG, 1:200; Advanced Immunochemical), anti-GFAP (rat IgG, 1:200; Invitrogen), antiadenomatous polyposis coli CC-1 (APC CC-1, mouse IgG, 1:200; Calbiochem), antihuman-specific nestin protein (rabbit IgG, 1:200, described previously, refs. 7–9), antiglutamate decarboxylase 67 (GAD67, mouse IgG, 1:200; Chemicon), antityrosine hydroxylase (TH, rabbit IgG, 1:200; Chemicon), anticholine acetyltransferase (ChAT, goat IgG, 1:50; Chemicon), antineurofilament 200 kDa (NF-H, mouse IgG, 1:200; Chemicon), anti–5-hydroxytrypamine (5HT, goat IgG, 1:200; Immunostar), antigrowth–associated protein (GAP43, mouse IgG, 1:1,000; Chemicon), anticalcitonin gene-related peptide (CGRP, rabbit IgG, 1:1,000; Affinity), antiplatelet endothelial cell adhesion molecule-1 (PECAM-1, rat IgG, 1:50; BD Bioscience Pharmingen), antivascular endothelial growth factor (VEGF, rabbit IgG, 1:50; Santa Cruz Biotechnology), anti-Bassoon (Bsn, mouse IgG, 1:200; Stressgen), antihuman-specific synaptophysin (hSyn, mouse IgG, 1:200; Chemicon), anti–K_i-67 (rabbit IgG, 1:500; Novocastra), and anti-alpha CaM kinase 2 (CaMK2a, mouse IgG, 1:100; Invitrogen).

For immunohistochemistry with anti-VEGF, -NF-H, -5HT, -GAP43, -CGRP, and -CaMK2a, we used a biotinylated secondary antibody (Jackson Immunoresearch Laboratory), after exposure to 0.3% H_2O_2 for 30 min at room temperature to inactivate the endogenous peroxidase. The signals were then enhanced with the Vectastain ABC kit (Vector Laboratories). Nuclei were stained with Hoechst 33258 (10 μg/mL; Sigma). Images were obtained by fluorescence microscopy (BZ-9000; Keyence) or with a confocal laser scanning microscope (LSM700; Carl Zeiss).

For immunoelectron microscopy, a preembedding peroxidase-conjugated immunoelectron microscopy technique was performed as described previously (10). Briefly, free-floating sections (40 μm thick) were prepared with a cryostat (CM3050; Leica). After being reacted with an anti-GFP antibody (rabbit IgG, 1: 100; MBL), the sections were incubated with peroxidase-conjugated goat antirabbit IgG for 1 h and fixed in 1% glutaraldehyde for 10 min. Staining for peroxidase was performed using 0.0125% 3,3′-diaminobenzidine tetrahydrochloride and 0.002% H_2O_2 in 0.05 mol/L Tris-HCl buffer (pH 7.6) for 10 min. Immunostained sections were further treated with OsO_4, dehydrated, and embedded in Epon 812. Ultrathin sections were cut with an ultramicrotome (Leica UC6; Leica Microsystems), stained quickly with lead citrate, and observed using a Hitachi electron microscope (H7100).

Quantitative Analyses of Stained Tissue Sections from the Engrafted Spinal Cord. To quantify cells of interest in H&E-stained, LFB-stained, and immunostained sections, we obtained images of the stained sections by fluorescence microscopy (BZ-9000; Keyence), manually outlined them, and quantified them using Dynamic cell count BZ-HIC software. The threshold values were maintained at a constant level for all analyses using BZ-HIC. For the spinal cord area quantification, we captured H&E images at the lesion epicenter and 0.9, 0.6, and 0.3 mm rostral and caudal

to the epicenter in axial sections at 100× magnification (n = 6, each). For the LFB$^+$ area quantification, we automatically captured four regions in axial sections, at the lesion epicenter and 0.9, 0.6, and 0.3 mm rostral and caudal to the epicenter at 400× magnification (n = 6, each). To quantify the NF-H$^+$ fibers, the midsagittal sections were scanned and tiled transversely at the lesion epicenter, and at 4 mm rostral and caudal to the epicenter at 400× magnification (n = 4, each). To quantify the 5HT$^+$ fibers, we automatically captured five regions in axial sections of the lumbar intumescence (6–8 mm caudal from the lesion epicenter) at 400× magnification [n = 6 each for the 7 d and control 56 d after SCI groups, and n = 5 in the human-induced pluripotent stem cell-derived neurospheres (hiPSC-NS) (56 d after SCI) group]. To quantify the GAP43$^+$ fibers, we captured the ventral regions in midsagittal sections 1 mm caudal to the epicenter at 400× magnification (n = 4, each). To quantify the CGRP$^+$ fibers, bilateral laminae Ш areas were captured in axial sections 4 mm rostral and caudal to the epicenter at 400× magnification (n = 4, each). To quantify the CaMK2a$^+$ fibers, the dorsal corticospinal tract (CST) areas were captured in axial sections of the lesion epicenter (Th10 level) at 400× magnification (n = 5, each). To quantify the VEGF$^+$ areas, we automatically captured four regions in axial sections at the lesion epicenter at 400× magnification (n = 4, each). To quantify the proportion of each cell phenotype in vivo, we selected representative midsagittal sections and automatically captured five regions within 1,000 μm rostral and caudal to the lesion epicenter at 200× magnification. Venus$^+$-engrafted and phenotypic marker-positive cells were counted in each section (n = 4 at 56 d after SCI and n = 5 at 112 d after SCI). The number of PECAM-1$^+$ blood vessels was manually counted in axial sections of the lesion epicenter at 100× magnification (n = 4, each).

RNA Isolation and RT-PCR. Differential expression in the epicenter segments of Th10-injured, nonobese diabetic-severe combined immunodeficient (NOD-SCID) mice was assessed 14 d post-injury. This time point revealed the gene-expression profile of the spinal cord 5 d after hiPSC-NS transplantation or PBS injection (n = 3, each). For human factors, the data are expressed as the amount of mRNA relative to that of cultured hiPSC-NSs before transplantation (n = 3). The mRNA levels of trophic factors were analyzed by quantitative RT-PCR arrays using TaqMan Array Fast (Applied Biosystems), following the manufacturer's instructions. Dissected spinal cord and hiPSC-NSs were rapidly frozen and placed in TRIzol (Invitrogen). The subsequent RNA isolation was performed according to the manufacturer's instructions. Total RNA (0.5 μg) was treated with TURBO DNase (Ambion) and then reverse transcribed with oligo (dT) primer and SuperScript III (Invitrogen). The quantitative mRNA expression of trophic factor-related genes was simultaneously analyzed (n = 3, each). The amount of cDNA was normalized to the *β-glucuronidase* (*Gusb*) mRNA. We used the following manufactured primers (Applied Biosystems) against human DNA sequences: GUSB-Hs99999908_m1, VEGFA-Hs00900054_m1, VEGFB-Hs0095798-0_g1, VEGFC-Hs01099206_m, NGF-Hs01113193_m1, BDNF-Hs00380947_m1, HGF-Hs00900066_m1, and GDNF-Hs0105532-9_m1 and the following manufactured primers (Applied Biosystems) against mouse DNA sequences: Gusb-Mm00446953_m1, Vegfa-Mm01281447_m1, Vegfb-Mm00442100_g1, Vegfc-Mm012-02432_m1, Ngf-Mm00443039_m1, Bdnf-Mm01334044_m1, Hgf-Mm01135184_m1, Cntf;Zfp91-Cntf-Mm00446373_m1, and Ntf3-Mm01182924_m1.

Statistical Analysis. An unpaired two-tailed Student's t test was used to assess the hiPSC-NS differentiation efficacy. One-way ANOVA followed by the Turkey–Kramer test for multiple comparisons was used for the H&E, LFB, PECAM-1, VEGF, NF-H, 5HT, GAP43, CGRP, Ki67, Rotarod, and DigiGait analyses. Repeated-measures two-way ANOVA, followed by the Turkey–Kramer test, was used for the BMS analysis. $^*P < 0.05$, $^{**}P < 0.01$.

1. Basso DM, et al. (2006) Basso Mouse Scale for locomotion detects differences in recovery after spinal cord injury in five common mouse strains. *J Neurotrauma* 23: 635–659.
2. Okada S, et al. (2004) Blockade of interleukin-6 receptor suppresses reactive astrogliosis and ameliorates functional recovery in experimental spinal cord injury. *J Neurosci Res* 76:265–276.
3. Ito M, et al. (2009) Type I interferon inhibits astrocytic gliosis and promotes functional recovery after spinal cord injury by deactivation of the MEK/ERK pathway. *J Neurotrauma* 26:41–53.
4. Li S, Kim JE, Budel S, Hampton TG, Strittmatter SM (2005) Transgenic inhibition of Nogo-66 receptor function allows axonal sprouting and improved locomotion after spinal injury. *Mol Cell Neurosci* 29:26–39.
5. Springer JE, et al. (2010) The functional and neuroprotective actions of Neu2000, a dual-acting pharmacological agent, in the treatment of acute spinal cord injury. *J Neurotrauma* 27:139–149.
6. Ito Z, et al. (2010) N-acetylglucosamine 6-O-sulfotransferase-1-deficient mice show better functional recovery after spinal cord injury. *J Neurosci* 30:5937–5947.
7. Iwanami A, et al. (2005) Transplantation of human neural stem cells for spinal cord injury in primates. *J Neurosci Res* 80:182–190.
8. Nakamura Y, et al. (2003) Expression of tubulin beta II in neural stem/progenitor cells and radial fibers during human fetal brain development. *Lab Invest* 83:479–489.
9. Kanemura Y, et al. (2002) Evaluation of in vitro proliferative activity of human fetal neural stem/progenitor cells using indirect measurements of viable cells based on cellular metabolic activity. *J Neurosci Res* 69:869–879.
10. Ogawa Y, et al. (2002) Transplantation of in vitro-expanded fetal neural progenitor cells results in neurogenesis and functional recovery after spinal cord contusion injury in adult rats. *J Neurosci Res* 69:925–933.

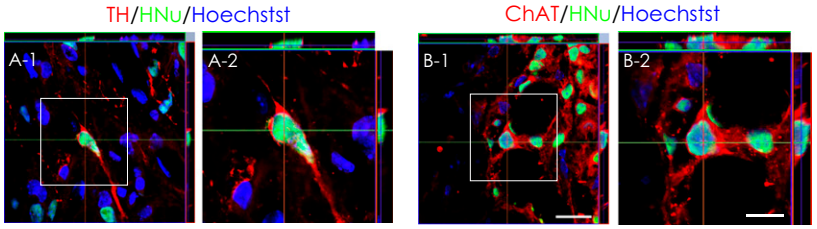

Fig. S1. Transplanted hiPSC-NS–derived cells differentiated into small numbers of TH$^+$ neurons and ChAT$^+$ cholinergic neurons. (*A* and *B*) TH$^+$/Venus$^+$ (dopaminergic) neurons and ChAT$^+$/Venus$^+$ (cholinergic) neurons were observed, but they were rare. (Scale bar, 20 μm in *A-1* and *B-1*; 10 μm in *A-2* and *B-2*.)

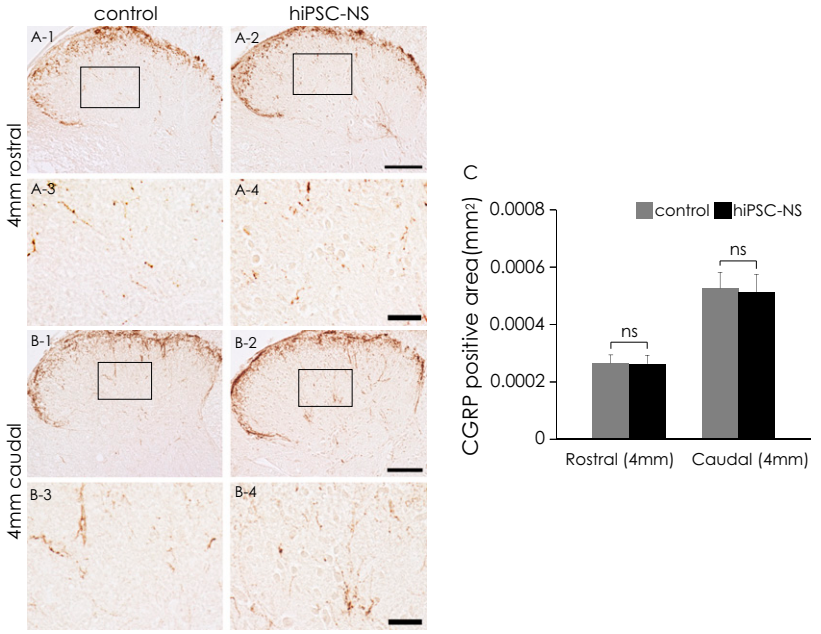

Fig. S2. Transplanted hiPSC-NSs did not induce abnormal innervations of pain-related CGRP$^+$ afferents after SCI. (*A*) Representative images of CGRP$^+$ fibers in lamina III, 4 mm rostral to the lesion epicenter. *A-3* and *A-4* show magnified images of the boxed areas in *A-1* and *A-2*, respectively. (*B*) Representative images of CGRP$^+$ fibers in lamina III 4 mm caudal to the lesion epicenter. *B-3* and *B-4* show magnified images of the boxed area in *B-1* and *B-2*, respectively. (*C*) Quantitative analysis of the CGRP$^+$ area in lamina III 4 mm rostral and caudal to the lesion epicenter. Values are means ± SEM (n = 4). (Scale bars, 100 μm in *A-1*, *A-2*, *B-1*, and *B-2*; 25 μm in *A-3*, *A-4*, *B-3*, and *B-4*.)

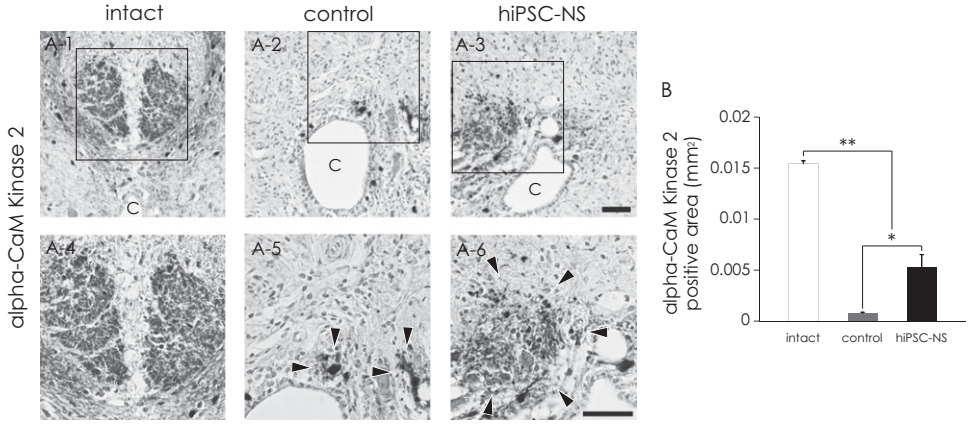

Fig. S3. Spared descending motor axons after SCI. (*A*) Representative images of alpha-CaM kinase 2 (CaMK2a)$^+$ descending motor axons in the dorsal corticospinal tract (CST) area of the lesion epicenter (Th10 level). *A-4*–*A-6* show magnified images of the boxed areas in *A-1*–*A-3*, respectively. (*B*) Quantitative analysis of the CaMK2a$^+$ area in the lesion epicenter (Th10 level). Note the presence of spared CaMK2a$^+$ fibers in the hiPSC-NS group. On the other hand, near complete axonal loss was observed in the control group. These findings were consistent with the electrophysiology results. Values are means ± SEM (n = 5). C, central canal of the spinal cord; arrowheads, CaMK2a$^+$ area. *P < 0.05, **P < 0.01. (Scale bars, 50 μm.)

Table S1. Summary of mice used in this study

	Exp1	Exp2	Exp3	Exp4	Exp5	Exp6	Exp7	Exp8	Total
hiPSC-NS group									
Transplantation	3	2	3	2	6 (3)	3	12 (2)	0	31 (5)
RNA 14 d	0	0	0	0	3	0	0	0	3
BMS 56 d	3	2	3	2	3	3	12	0	28
BMS 112 d	0	0	0	0	3	3	12	0	18
DigiGait 56 d	0	0	0	0	3	3	12	0	18
MEP 112 d	0	0	0	0	3	3	11 (1)	0	17 (1)
Rotarod 56 d	3	2	3	2	0	0	0	0	10
Histology 56 d	3	2	3	2	0	0	0	0	10
Histology 112 d	0	0	0	0	3	3	11	0	17
Control group									
Transplantation	3	2	2	3	0	8 (3)	0	11	29 (3)
RNA 14 d	0	0	0	0	0	2	0	1	3
BMS 56 d	3	2	2	3	0	6	0	10	26
BMS 112 d	0	0	0	0	0	6	0	10	16
DigiGait 56 d	0	0	0	0	0	6	0	10	16
MEP 112 d	0	0	0	0	0	5 (1)	0	10	15 (1)
Rotarod 56 d	3	2	2	3	0	0	0	0	10
Histology 56 d	3	2	2	3	0	0	0	0	10
Histology 112 d	0	0	0	0	0	5	0	10	15

Number of mice used (unplanned deaths).